Ultrasound Obstet Gynecol 2010; **36**: 218–225
Published online 13 July 2010 in Wiley InterScience (www.interscience.wiley.com). **DOI:** 10.1002/uog.7643

Ultrasonic attenuation estimation of the pregnant cervix: a preliminary report

B. L. McFARLIN*, T. A. BIGELOW†, Y. LAYBED†, W. D. O'BRIEN Jr‡, M. L. OELZE‡ and J. S. ABRAMOWICZ§

**Women, Children and Family Health Science, University of Illinois at Chicago and §Obstetrics and Gynecology, Rush University Medical Center, Chicago and ‡Computer and Electrical Engineering, University of Illinois at Urbana-Champaign, Urbana, IL and †Electrical and Computer Engineering, Iowa State University, Ames, IA, USA*

KEYWORDS: attenuation; cervical length; cervical ripening; detection of cervical ripening; preterm birth

ABSTRACT

Objective *Estimates of ultrasonic attenuation (the loss of energy as an ultrasonic wave propagates through tissue) have been used to evaluate the structure and function of tissues in health and disease. The purpose of this research was to develop a method to estimate ultrasonic cervical attenuation during human pregnancy using a clinical ultrasound system.*

Methods *Forty women underwent a cervical scan once during pregnancy with the Zonare® z.one clinical ultrasound system using a 4–9-MHz endovaginal transducer. This ultrasound system provides access to radiofrequency (RF) image data for processing and analysis. In addition, a scan of a tissue-mimicking phantom with a known attenuation coefficient was acquired and used as a reference. The same settings and transducer used in the clinical scan were used in the reference scan. Digital data of the beam-formed image were saved in Digital Imaging and Communications in Medicine (DICOM) format on a flash drive and converted to RF data on a personal computer using a Matlab® program supplied by Zonare. Attenuation estimates were obtained using an algorithm that was independently validated using tissue-mimicking ultrasonic phantoms.*

Results *RF data were acquired and analyzed to estimate attenuation of the human pregnant cervix. Regression analysis revealed that attenuation was: a predictor of the interval from ultrasound examination to delivery ($\beta = 0.43$, $P = 0.01$); not a predictor of gestational age at time of examination ($\beta = -0.23$, $P = 0.15$); and not a predictor of cervical length ($\beta = 0.077$, $P = 0.65$).*

Conclusions *Ultrasonic attenuation estimates have the potential to be an early and objective non-invasive method to detect interval between examination and delivery. We hypothesize that a larger sample size and a longitudinal study design will be needed to detect gestational age-associated changes in cervical attenuation. Copyright © 2010 ISUOG. Published by John Wiley & Sons, Ltd.*

INTRODUCTION

Preterm birth is a leading cause of infant morbidity and mortality worldwide. Assessment of uterine contractility and cervical change by digital examination have been considered to be a method to diagnose preterm labor[1]. Since the introduction of tocolytics, preterm birth rates have not been reduced[2–5] and the medications carry significant maternal and fetal risks[2,6–9]. Evidence suggests that ripening of the cervix precedes uterine contractions and subsequent delivery of the fetus[10,11]. Cervical ripening is a process characterized by collagen disorganization[12–14], decreased collagen concentration and increased water content[13–19]. A ripened cervix, with loss of the mucus barrier, may be the initial mechanism leading to a cascade of events (increased inflammation, production of cytokines and enzymes, and loss of cervical mucus) that result in preterm birth[20–22]. Thus, maintaining a closed unripe cervix with an intact cervical mucus barrier during pregnancy is critical for preventing preterm birth. Cervical changes that occur before preterm birth go undetected because women do not have symptoms (contractions) or signs (vaginal discharge)[11,23]. Measurement of early cervical changes (increased collagen disorganization and decreased collagen concentration) associated with remodeling of the extracellular matrix then becomes a medically significant milestone that may predict preterm labor and birth.

There is considerable interest in developing new imaging techniques to accurately predict cervical changes associated with full-term and preterm labor[1,24–26].

Correspondence to: Dr B. L. McFarlin, University of Illinois at Chicago, Room 858 M/C 802, 845 S. Damen Ave., Chicago, IL 60612, USA (e-mail: bmcfar1@uic.edu)

Accepted: 13 November 2009

Cervical shortening and dilation can be detected using clinical ultrasound systems. However, an objective non-invasive ultrasonic method to determine tissue property changes (increased collagen disorganization and water concentration) associated with cervical ripening does not exist. Estimates of ultrasonic attenuation (the loss of energy as an ultrasonic wave propagates through tissue)[27] have been used to evaluate the structure and function of tissues in health and disease[28–36]. Attenuation has been observed to be related to tissue stiffness, collagen concentration and water concentration[28–31,37]. During pregnancy, as the collagen-rich cervix prepares for labor and birth, the cervix transforms from a rigid structure to a soft, extensible structure. It is thus hypothesized that by estimating changes in ultrasonic attenuation, these dynamic changes in tissue structure and function can be detected.

Our previous work in an animal model demonstrated that the decreased collagen concentration associated with cervical ripening clearly affected ultrasonic attenuation in cervical tissue[18]. We found that estimates of attenuation corresponded to gestational age changes in the rat cervix as ripening occurred[18]. In the rat cervix, attenuation was greater in the non-pregnant cervix and at an early gestational age, and decreased as pregnancy advanced towards full-term[18]. We attributed those changes in attenuation to changes in collagen disorganization[13,18]. Figure 1 presents atomic force microscopy images of a non-pregnant rat cervix, showing tightly packed and organized collagen bundles, and a day-21 pregnant rat cervix (the day on which rats typically deliver), showing highly disorganized collagen. Similar changes in collagen disorganization occur in human pregnancy as the cervix ripens[38]. We postulate that the development of methods to detect cervical attenuation in human pregnancy might be a useful means of estimating cervical tissue-property changes associated with cervical ripening.

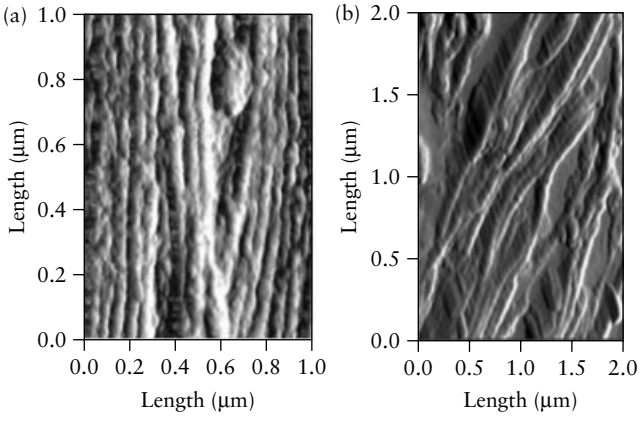

Figure 1 Atomic force microscopy images of the cervix from (a) a non-pregnant rat, displaying highly organized, pack bundles of collagen and (b) a cervix on day 21 of pregnancy, displaying disorganized collagen with space between the fibrils. The bundles of collagen that are displayed in these images are < 0.1 μm. Rats typically deliver on day 21. (Image by R. Bhargava, W. King, UIUC, and B. L. McFarlin, UIC).

Recently, a clinical ultrasound system (z.one; Zonare® Medical Systems, Inc., Mountain View, CA, USA) became available that allows access to radiofrequency (RF) image data of the human pregnant cervix similar to our previous animal studies[18,39]. Our previous studies in the animal model used ultrasound research data-acquisition systems (Panametrics, Waltham, MA, USA) and single-element high-frequency transducers (35 and 65 MHz)[18,39]. We wanted to extend our previous work, namely detecting cervical tissue changes in the animal model, to those changes occurring in human pregnancy by estimating ultrasonic attenuation of the human pregnant cervix with a clinical ultrasound system using a phased-array transducer. The purpose of this study was to develop a method to estimate ultrasonic attenuation in the human pregnant cervix using a clinical ultrasound system that provided access to RF image data for processing and analysis.

METHODS

Forty women underwent a cervical ultrasound examination once during pregnancy, using the z.one clinical ultrasound system. No longitudinal assessments of cervical attenuation were conducted on the women who participated in the study. The gestational age at the time of the cervical ultrasound examination ranged from 10 to 41 weeks. The inclusion criteria were: women with a live intrauterine pregnancy of between 10 and 42 weeks of gestation; and willingness to participate in the study. Women with a cerclage, who had undergone a loop electrosurgical excision procedure (LEEP) or a cone biopsy, or who had experienced rupture of membranes, vaginal bleeding or a fetal death, were excluded from the study.

All ultrasound data were acquired by one investigator (B.L.M.) with the same system presets for each examination. Two sagittal scans of the cervix, which included visualization of the internal and external os, were acquired for each woman using a 4–9-MHz (6.8-MHz center frequency) endovaginal transducer. Attenuation estimates and cervical length measurements were conducted for each of the two images on each woman's cervix. Care was taken to obtain the scan in the same manner each time. Cervical length was measured, from the internal os to the external os, on the same image on which data would be analyzed for ultrasound attenuation. In addition, a scan of a tissue-mimicking phantom (University of Wisconsin, Madison, WI, USA), acquired with the same 4–9-MHz endovaginal transducer, was used to obtain the reference ultrasound signal for use when estimating cervical attenuation. The tissue-mimicking phantom was custom-made using 45- to 53-μm glass beads in agar and has been well characterized[40] and used to obtain reference ultrasound data for research at the Bioacoustics Research Laboratory at the University of Illinois at Urbana-Champaign (Urbana, IL, USA). The attenuation coefficient of the tissue-mimicking phantom was

0.64 dB/cm-MHz and varied by as much as 0.15 dB/cm-MHz when evaluated among eight ultrasound research laboratories[40]. Figure 2 displays an ultrasound image of a tissue-mimicking phantom obtained with the 4–9-MHz endovaginal transducer used in this study. The mean attenuation of the phantom, measured using the endovaginal transducer, was 0.64 dB/cm-MHz (± 0.13 dB/cm-MHz). The settings of the ultrasound system were identical between the human scan and the reference phantom scan. The performance characteristics of the Zonare Medical Systems 4–9-MHz endovaginal transducer are summarized in Table 1.

Digital Imaging and Communications in Medicine (DICOM) data of the beam-formed image were saved on a flash drive and converted to RF data on a personal computer using a Matlab® (Mathworks, Natick, MA, USA) program supplied by Zonare. Gestational age of the fetus was determined from the first-trimester ultrasound examination. Cervical length was measured at the time of the examination. Pregnancy characteristics and previous history of preterm birth were collected via patient interview. None of the women was subjected to a digital examination of the cervix. Gestational age at delivery and neonatal outcome data were acquired by telephone verbal report from the patient because most of the women delivered at various institutions throughout the states of Illinois and Indiana. All of the women were cognisant of infant birth weight, Apgar scores and date of delivery.

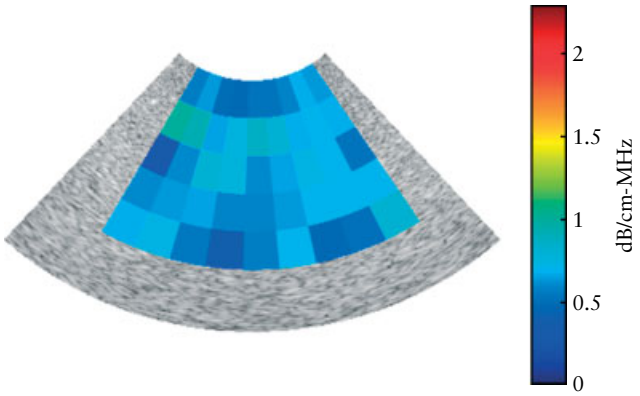

Figure 2 Attenuation map for a B-mode image obtained from the tissue-mimicking phantom (the phantom has a known attenuation coefficient of 0.64 dB/cm-MHz) using a 4–9-MHz endovaginal transducer (z.one; Zonare Medical Systems, Inc.). Each pixel represents a mean attenuation coefficient value for a region of interest. The mean (± SD) attenuation coefficient measured for the phantom was 0.64 (± 0.13) dB/cm-MHz.

Table 1 Transducer performance characteristics as reported by Zonare Medical Systems, Inc

Transducer property	*Endovaginal 4–9 MHz*
Number of elements	128
Center frequency (6 dB)	6.4 MHz (± 0.2)
Bandwidth	≥ 65%
Focal length	33 mm (± 10)
Pulse width (6 dB)	≤ 0.24 μs

The attenuation estimates were obtained using an algorithm that was previously validated in tissue-mimicking ultrasound phantoms[41]. Briefly, backscattered RF waveforms were obtained from an unknown sample and from a reference phantom with a known attenuation coefficient, using the same transducer and system settings. Attenuation is defined as the loss of signal amplitude with depth as a function of frequency, and attenuation coefficient is the attenuation normalized to distance and/or frequency. The power spectra of both the reference phantom and the unknown sample are functions of frequency and propagation depth in the sample. The frequency dependence of the power spectra depends on the system transfer function, attenuation, scattering and diffraction of sound waves. The system transfer function and the diffraction term are approximated to be the same for both the reference sample and the phantom and can be eliminated by dividing the power spectra from the two samples and taking the logarithm. Determining the rate of change with depth into the tissue of this ratio for each frequency eliminates the scattering terms, assuming that the scattering properties do not vary with depth over the region of interest (ROI). Averaging the remaining coefficients with respect to frequency, and adding the attenuation coefficient of the reference phantom, then gives an estimate of the attenuation coefficient (dB/cm-MHz) in the unknown sample.

One investigator (B.L.M.) chose the ROIs for obtaining attenuation estimates. The ROIs were chosen based upon adequate size of ROI in homogeneous tissue (no cystic areas or amniotic fluid). Because of the tissue architecture, the same ROI could not be sampled in each image. Therefore, we used one attenuation estimate value for each patient. The investigators processing the RF data (T.A.B. and Y.L.) were blinded to gestational age and clinical information about the patients. In order to obtain an error of less than 10%, the ROI must be at least 40 wavelengths (1 cm in length for a 6-MHz transducer) and contain at least 30 beam lines. Institutional Review Board approval of the study was obtained at Rush University and at the University of Illinois at Chicago.

The purpose of this study was to develop methodology to estimate attenuation using a clinical ultrasound system. Hence, the study was not powered to detect differences in attenuation and cervical length as a function of gestational age at the time of examination. However, descriptive statistics and one-way analysis of variance (ANOVA) (two-tailed tests) were calculated for gestational age at the time of examination (SPSS 16.0; SPSS, Chicago, IL, USA). Scatterplots with linear regression lines and 95% CI were calculated to display the relationship between attenuation and interval to delivery, cervical length and gestational age at the time of examination. An alpha level of 0.05 was used for all statistical tests.

RESULTS

Forty women participated in the study. Seven women delivered at < 37 weeks of gestation. Table 2 displays the characteristics of women in the study. Regression analysis revealed that attenuation was: (1) a predictor of the interval from ultrasound examination to delivery ($\beta = 0.43$, $P = 0.011$); (2) not a predictor of gestational age at time of examination ($\beta = -0.23$, $P = 0.15$); and (3) not a predictor of cervical length ($\beta = 0.077$, $P = 0.65$). Figure 3 displays scatterplots of cervical-attenuation estimates as a function of interval from ultrasound examination to delivery, gestational age at time of examination and cervical length, for the women in the study. Table 3 displays the characteristics of the women in the study who delivered preterm. Figure 2 displays the attenuation coefficient of the tissue-mimicking phantom (mean = 0.64 dB/cm-MHz, SD = 0.13 dB/cm-MHz). Similar attenuation estimate results were reported by other investigators who used this phantom[40].

Table 4 summarizes the characteristics of women who had a cervical length of < 2.5 cm at the time of the ultrasound examination. Patient no. 35 had a very short cervix, a moderate attenuation value and did not deliver for 11 more weeks. She was monitored and did not receive tocolytics as she was not contracting. Patient no. 41 was noted to have a cervical length of 2.26 cm at 18 weeks, a moderately high attenuation value and did not deliver for 19 more weeks. Figure 4 displays images of the cervices of two women who participated in the study – one at 14 weeks of gestation and one at 38 weeks of gestation. Ultrasound B-mode images of the cervices (Figures 4a and c) of the two women were created along with corresponding superimposed maps of the attenuation estimates for the cervices (Figures 4b and d). Each pixel in the superimposed image represents a mean attenuation value for the intended ROI of the cervix. We wanted to evaluate both the internal and external portions of the cervix, but this was not always possible because of inhomogeneities and architecture variances of the cervical tissue. In the two cases presented in Figure 4, mean attenuation was greater in the 14-week cervix than in the 38-week cervix, although there was little change in cervical length measurements (3.1 cm for the 14-week cervix and 3.5 cm for the 38-week cervix).

Like the cervical attenuation estimates in our previous animal studies[18,39], considerable between-subject attenuation variability was noted (Figure 3a). Unlike attenuation estimates in the previous animal cervical studies, however, the attenuation variability across the cervix for a specific patient was reduced compared with that in rats as a result of the larger ROIs sampled in the larger human cervix.

Table 2 Characteristics of the 40 study participants

Variable	*All women* (n = 40)	*Women delivering at ≥ 37 weeks* (n = 33)	*Women delivering at < 37 weeks* (n = 7)
Maternal age (years)	28 ± 6.7 (19–42)	28 ± 6.8 (19–42)	28 ± 8.4 (19–38)
Gravidity	2 (1–5)	2 (1–5)	2 (1–4)
History of PTL	7	1	6
History of PTD	7	1	6
GA at ultrasound (weeks)	22.5 ± 8.6 (10–40)	22.8 ± 8.9 (10–40)	23.4 ± 8.1 (12–35)
Attenuation (dB/cm-MHz)	1.19 ± 0.36 (0.31–1.9)	1.24 ± 0.31 (0.56–1.9)	1.06 ± 0.48 (0.31–1.62)
Interval from ultrasound to delivery (weeks)	14.6 ± 8.7 (0–29)	15.8 ± 8.2 (0–29)	9.4 ± 9.3 (1–24)
Cervical length (cm)	3.7 ± 1.32 (0.56–6.1)	3.8 ± 1.33 (0.56–6.1)	2.9 ± 1.53 (0.74–5.1)
GA at delivery (weeks)	37.6 ± 3.1 (27–41)	38.8 ± 1.1 (37–41)	32.5 ± 3.8 (27–36)
Birth weight (g)	2970 ± 7.95 (843–4223)	3224 ± 475 (2300–4223)	1891 ± 849 (843–3288)

Data are expressed as *n*, mean ± SD (range) or median (range). GA, gestational age; PTD, preterm delivery (< 37 weeks); PTL, preterm labor (< 37 weeks).

Table 3 Characteristics of the seven study participants who delivered preterm

Patient no.	*Gravidity*	*Parity (FPAL)*	*History of preterm birth*	*GA at ultrasound (weeks)*	*GA at delivery (weeks)*	*Cervical length (cm)*	*Mean attenuation (dB/cm-MHz)*
2	1	0000	No	35	36	2.63	0.55
4	2	0010	No	32	34	3.06	1.62
17	2	0101	Yes	12	36	4.89	1.23
19	4	1021	No	24	27	2.97	0.316
32	2	1001	No	26	28	3.10	1.49
33	1	0000	No	13	36	5.10	1.21
30	3	2002	No	23	34	1.24	1.06

FPAL, full-term, preterm, abortion, living; GA, gestational age.

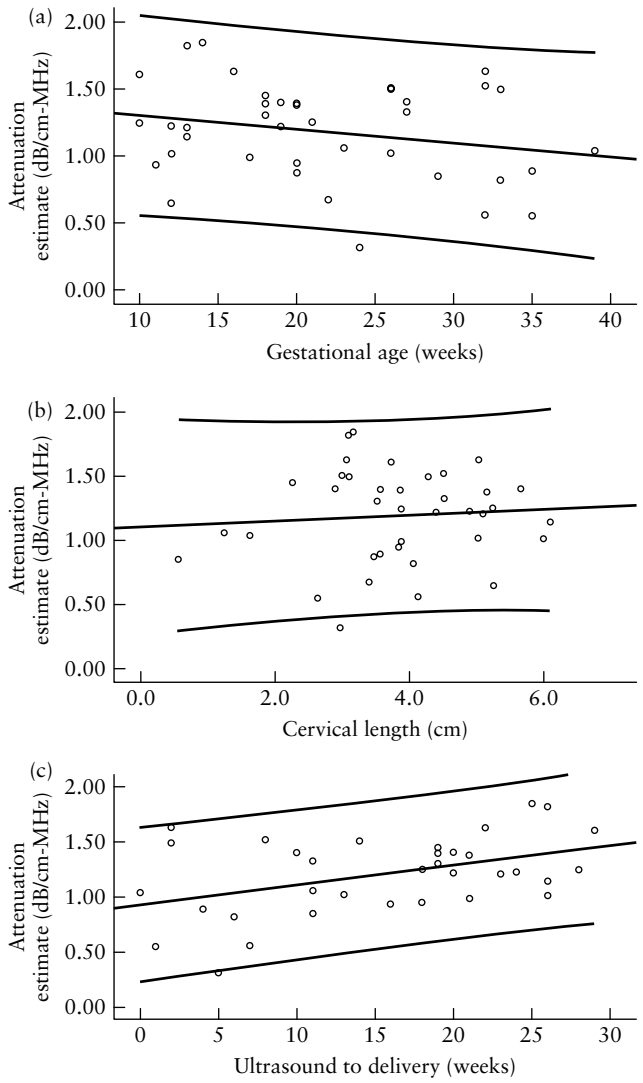

Figure 3 Scatterplots of ultrasonic attenuation coefficient estimates of the cervix in relation to gestational age at the time of ultrasound examination (a), cervical length (b) and time between ultrasound examination and delivery (c), showing linear regression lines and 95% CIs. (a) A trend of decreasing attenuation as pregnancy approached full term (≥ 37 weeks gestation) was observed ($P = 0.15$). Linear regression equation: $y = -0.01\,x + 1.41$; $R^2 = 0.055$. (b) The relationship between cervical attenuation coefficient estimates and cervical length was not significant ($P = 0.65$). Linear regression equation: $y = 0.022\,x + 1.10$; $R^2 = 0.006$. (c) Attenuation significantly predicted interval to delivery. Women with lower cervical attenuation estimates delivered significantly earlier than women with higher cervical attenuation estimates ($P = 0.011$). Linear regression equation: $y = 0.018\,x + 0.932$; $R^2 = 0.100$.

DISCUSSION

The results of this study demonstrate that we were able to acquire and analyze useable RF data to yield estimates of local attenuation in the human pregnant cervix. Local ultrasonic attenuation has been successfully used to characterize the structure and health of biological tissues. Applications have included diagnosing diffuse liver disease[42–45], monitoring tissue changes after high-intensity ultrasound therapy[46], assessing changes in the liver following prednisone treatment[47], differentiating between benign and malignant tissue in the prostate[48] and assessing the mineral content of bone[49–52]. Attenuation of tissue has been observed to decrease significantly as water concentration increases and density decreases[53,54]. With the dynamic changes in cervix microstructure (increased collagen disorganization and decreased collagen concentration) and water concentration during the ripening process, it is reasonable to consider using attenuation to detect changes in the cervix that are associated with cervical ripening. Our own research in the rat cervix observed significant decreases in attenuation as pregnancy progressed towards full-term[18], as well as significant correlations of attenuation with cervix tissue water concentration (*ex vivo* study: $r = 0.98$, $P < 0.001$)[18].

Significant between-subject variability in attenuation was observed. Our previous rat-cervix attenuation estimates also showed marked between- subject variability, even though the rat pregnancy gestational age is known to within 12 h of conception, suggesting biologic variation in cervical tissue starting points. These findings suggest that future longitudinal repeated-measure designs will be needed to detect cervical change leading to labor, as each patient may have her own cervix attenuation starting point. It is possible that the patterns of cervical change will be different in women delivering at full-term or at preterm. It is promising that in this small sample size, attenuation estimates were associated with interval to delivery. There may be a critical level of attenuation that corresponds to signaling of impending labor. Note that the cervical length in the Figure 4 images was not markedly different, but the attenuation values and gestational age were very different. The lack of relationship between cervical-attenuation estimates and cervical length suggests that the process of microstructural tissue property changes and cervical length may be independent of, or at least not concurrent with, attenuation.

Limitations

The goal of this research was to construct attenuation maps of the entire cervix, or at least be consistent in sampling the internal and external portions of the cervix. The attenuation algorithm assumes homogeneous tissue. We selected cervical ROIs that appeared to be homogeneous tissue, without any cystic areas. Because of the cervical tissue architecture, the same ROIs could not be uniformly sampled in each individual case. Therefore, we used one of the two cervical images we collected in each case to produce the results presented in this study. This undersampling of the cervix is a limitation of our approach given the natural inhomogeneity of the cervix. This also may have increased the between-subject variability because the same regions of the cervix were not compared in every case. In future studies, our goal will be to develop methods to obtain attenuation estimates throughout the entire cervix.

A further limitation of the study is that the attenuation estimation algorithm assumes that the ROI is

Table 4 Characteristics of the five study participants with a cervical length of < 2.5 cm at the time of examination

Patient no.	*Gravidity*	*Parity (FPAL)*	*History of preterm birth*	*GA at ultrasound (weeks)*	*GA at delivery (weeks)*	*Cervical length (cm)*	*Mean attenuation (dB/cm-MHz)*
35	2	0100	Yes	29	40	0.56	1.01
13	1	0000	No	38	38	0.94	0.65
30	3	2002	No	23	34	1.24	1.06
6	2	1010	No	39	40	1.62	1.04
41	2	0101	Yes	18	37	2.26	1.45

Results are ordered according to increasing cervical length. FPAL, fullterm, preterm, abortion, living; GA, gestational age.

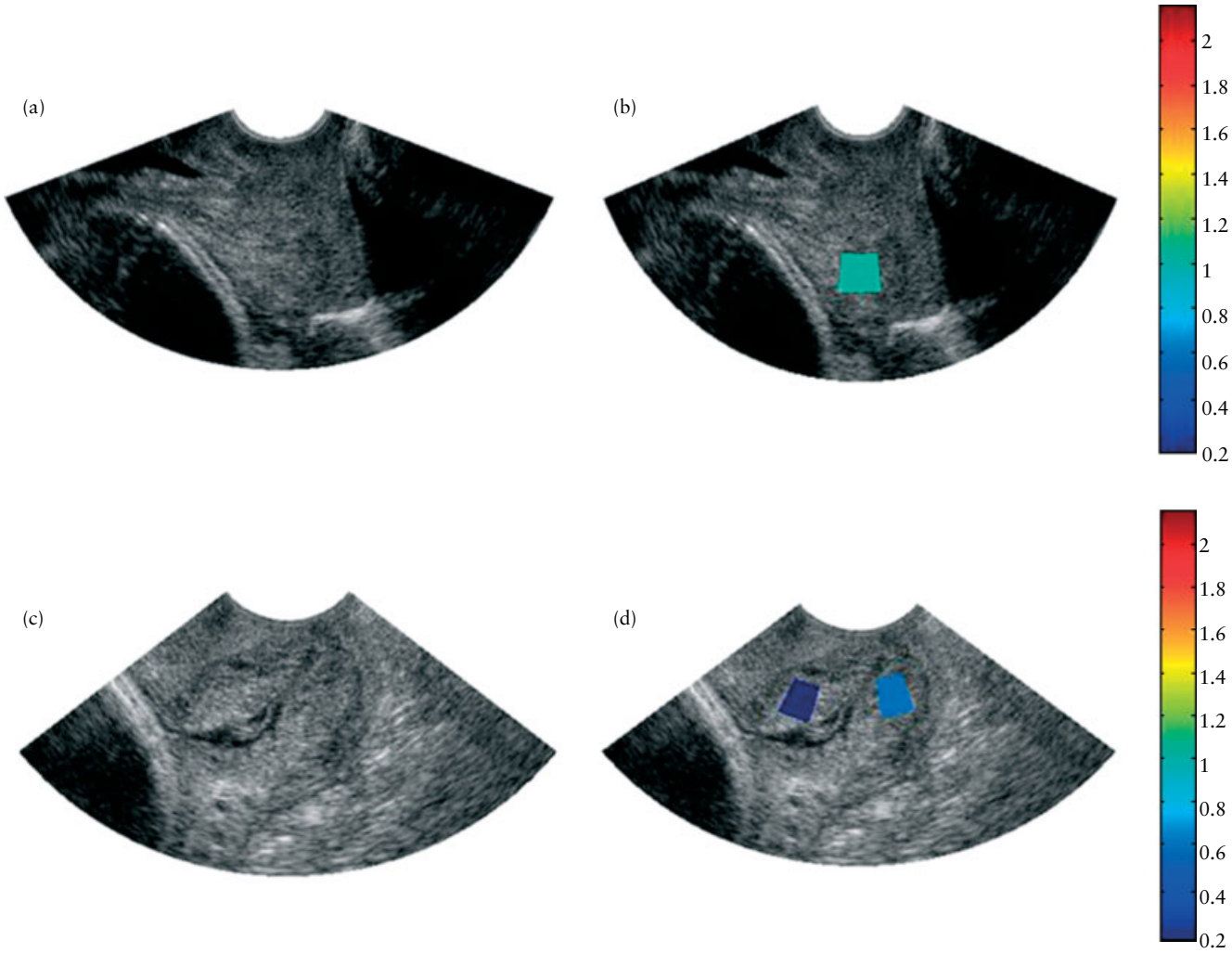

Figure 4 Ultrasound B-mode images (a,c) and B-mode images superimposed with maps of the mean attenuation estimates (b,d) of two women in the study, one at 14 weeks of gestation, with cervical length 31 mm (a,b) and the other at 38 weeks of gestation, with cervical length 35 mm (c,d). The colors of the regions of interest represent a mean attenuation (dB/cm-MHz) consistent with the corresponding scale bar.

homogeneous (i.e. has the same attenuation and scattering properties). Therefore inhomogeneities within the ROI could result in errors in the attenuation estimate. The best way to reduce these errors is to increase the ROI size. Because the minimal ROI size needed for accurate estimates is a function of wavelength, increasing the ultrasound frequency (reducing the wavelength) is a relatively simple approach for reducing the sensitivity to inhomogeneities. The smaller ROIs obtained at higher ultrasound frequencies could also enhance our ability to obtain attenuation estimates at late gestational ages when the cervix has a shorter length as a result of effacement[42].

The small sample size of this study limits the generalizability of our findings. We are encouraged by our preliminary findings that it may be possible to detect early cervical tissue property changes in human pregnancy that lead to labor. In the future, we plan to conduct studies with longitudinal repeated-measures designs to assess cervical

attenuation throughout pregnancy as a measure of the cervix preparing for labor.

Conclusions

It is clear that we still have much to learn about the mechanisms and processes of cervical ripening[1]. New imaging technologies are necessary to fully understand and detect such changes during pregnancy[1]. Significant technological advances in computing and instrumentation have made it possible to improve the detection of tissue-property changes associated with cervical ripening[18,25,26,39,55–62]. We postulate that it will be possible to add attenuation assessment processing software to current clinical ultrasound systems with RF data capabilities. Attenuation estimates have the potential to be an early and objective non-invasive method of detecting changes in cervical tissue microstructure that are consistent with cervical ripening.

ACKNOWLEDGMENTS

This project was supported by the University of Illinois at Chicago (UIC) Center for Clinical and Translational Science (CCTS) K12 award (B.L.M.), which was funded, in part, by the National Center for Research Resources, National Institutes of Health grant UL1RR029879; Zonare® Medical Systems, Inc. (ultrasound system loan), NIH grant R01 CA111289 (W.D.O.) and Rush University Medical Center, Department of Obstetrics and Gynecology.

REFERENCES

1. Rozenberg P. The secret cervix. *Ultrasound Obstet Gynecol* 2008; **32**: 126–127.
2. Caritis S. Adverse effects of tocolytic therapy. *BJOG* 2005; **112** (Suppl 1): 74–78.
3. Goldenberg RL. The management of preterm labor. *Obstet Gynecol* 2002; **100**: 1020–1037.
4. Iams JD. The role of tocolysis in the prevention of preterm birth. *Birth* 1996; **23**: 40–41.
5. Iams JD. The epidemiology of preterm birth. *Clin Perinatol* 2003; **30**: 651–664.
6. Friedman DM, Blackstone J, Young BK, Hoskins IA. Fetal cardiac effects of oral ritodrine tocolysis. *Am J Perinatol* 1994; **11**: 109–112.
7. Friedman S, Flidel-Rimon O, Steinberg M, Shinwell ES. Indomethacin tocolysis and white matter injury in preterm infants. *J Matern Fetal Neonatal Med* 2005; **18**: 87–91.
8. Koontz SL, Friedman SA, Schwartz ML. Symptomatic hypocalcemia after tocolytic therapy with magnesium sulfate and nifedipine. *Am J Obstet Gynecol* 2004; **190**: 1773–1776.
9. Samol JM, Lambers DS. Magnesium sulfate tocolysis and pulmonary edema: the drug or the vehicle? *Am J Obstet Gynecol* 2005; **192**: 1430–1432.
10. Mahendroo MS, Porter A, Russell DW, Word RA. The parturition defect in steroid 5alpha-reductase type 1 knockout mice is due to impaired cervical ripening. *Mol Endocrinol* 1999; **13**: 981–992.
11. Vidaeff AC, Ramin SM. From concept to practice: the recent history of preterm delivery prevention. Part I: cervical competence. *Am J Perinatol* 2006; **23**: 3–13.
12. Clark K, Ji H, Feltovich H, Janowski J, Carroll C, Chien EK. Mifepristone-induced cervical ripening: structural, biomechanical, and molecular events. *Am J Obstet Gynecol* 2006; **194**: 1391–1398.
13. Feltovich H, Ji H, Janowski JW, Delance NC, Moran CC, Chien EK. Effects of selective and nonselective PGE2 receptor agonists on cervical tensile strength and collagen organization and microstructure in the pregnant rat at term. *Am J Obstet Gynecol* 2005; **192**: 753–760.
14. Leppert PC, Kokenyesi R, Klemenich CA, Fisher J. Further evidence of a decorin-collagen interaction in the disruption of cervical collagen fibers during rat gestation. *Am J Obstet Gynecol* 2000; **182**: 805–811.
15. Danforth DN, Buckingham JC, Roddick JW Jr. Connective tissue changes incident to cervical effacement. *Am J Obstet Gynecol* 1960; **80**: 939–945.
16. Eckman G, Almstrom H, Gramstrom L, Malmstrom A, Norman M, Woessner JF Jr. Connective tissue in human cervical ripening. In *The Extracellular Matrix of the Uterus, Cervix and Fetal Membranes: Synthesis, Degradation and Hormonal Regulation*, Leppert PC, Woessner JF Jr (eds). Perinatology Press: Ithica, NY, 1991; 87–104.
17. Golichowski AM, King SR, Mascaro K. Pregnancy related changes in rat cervical glycosaminoglycans. *Biochem J* 1980; **192**: 1–8.
18. McFarlin BL, O'Brien WDJ, Oelze ML, Zachary JF, White-Traut RC. Quantitative ultrasound assessment of the rat cervix. *J Ultrasound Med* 2006; **25**: 1031–1040.
19. Yu SY, Leppert PC. The collagenous tissues of the cervix during pregnancy and delivery. In *The Extracellular Matrix of the Uterus, Cervix, and Fetal Membranes: Synthesis, Degradation and Hormonal Regulation*, Leppert PC, Woessner JF Jr (eds). Perinatology Press: Ithaca, NY, 1991; 68–76.
20. Gomez R, Romero R, Medina L, Nien JK, Chaiworapongsa T, Carstens M, Gonzalez R, Espinoza J, Iams JD, Edwin S, Rojas I. Cervicovaginal fibronectin improves the prediction of preterm delivery based on sonographic cervical length in patients with preterm uterine contractions and intact membranes. *Am J Obstet Gynecol* 2005; **192**: 350–359.
21. Hassan S, Romero R, Hendler I, Gomez R, Khalek N, Espinoza J, Nien JK, Berry SM, Bujold E, Camacho N, Sorokin Y. A sonographic short cervix as the only clinical manifestation of intra-amniotic infection. *J Perinat Med* 2006; **34**: 13–19.
22. Hassan SS, Romero R, Berry SM, Dang K, Blackwell SC, Treadwell MC, Wolfe HM. Patients with an ultrasonographic cervical length < or = 15 mm have nearly a 50% risk of early spontaneous preterm delivery. *Am J Obstet Gynecol* 2000; **182**: 1458–1467.
23. Vidaeff AC, Ramin SM. From concept to practice: the recent history of preterm delivery prevention. Part II: Subclinical infection and hormonal effects. *Am J Perinatol* 2006; **23**: 75–84.
24. Garfield RE, Chwalisz K, Shi L, Olson G, Saade GR. Instrumentation for the diagnosis of term and preterm labour. *J Perinat Med* 1998; **26**: 413–436.
25. Garfield RE, Maner WL, Maul H, Saade GR. Use of uterine EMG and cervical LIF in monitoring pregnant patients. *BJOG* 2005; **112** (Suppl 1): 103–108.
26. Tekesin I, Hellmeyer L, Heller G, Romer A, Kuhnert M, Schmidt S. Evaluation of quantitative ultrasound tissue characterization of the cervix and cervical length in the prediction of premature delivery for patients with spontaneous preterm labor. *Am J Obstet Gynecol* 2003; **189**: 532–539.
27. Shung KK, Smith MB, Tsui B. *Principles of Medical Imaging*. Academic Press: San Diego, CA, 1992.
28. Baldwin SL, Yang M, Marutyan KR, Wallace KD, Holland MR, Miller JG. Ultrasonic detection of the anisotropy of protein cross linking in myocardium at diagnostic frequencies. *IEEE Trans Ultrason Ferroelectr Freq Control* 2007; **54**: 1360–1369.
29. Hall CS, Dent CL, Scott MJ, Wickline SA. High-frequency ultrasound detection of the temporal evolution of protein cross

linking in myocardial tissue. *IEEE Trans Ultrason Ferroelectr Freq Control* 2000; **47**: 1051–1058.
30. Hall CS, Nguyen CT, Scott MJ, Lanza GM, Wickline SA. Delineation of the extracellular determinants of ultrasonic scattering from elastic arteries. *Ultrasound Med Biol* 2000; **26**: 613–620.
31. Hall CS, Scott MJ, Lanza GM, Miller JG, Wickline SA. The extracellular matrix is an important source of ultrasound backscatter from myocardium. *J Acoust Soc Am* 2000; **107**: 612–619.
32. Insana MF. Modeling acoustic backscatter from kidney microstructure using an anisotropic correlation function. *J Acoust Soc Am* 1995; **97**: 649–655.
33. Insana MF, Wood JG, Hall TJ. Identifying acoustic scattering sources in normal renal parenchyma in vivo by varying arterial and ureteral pressures. *Ultrasound Med Biol* 1992; **18**: 587–599.
34. O'Brien WD, Sagar KB, Warltier DC, Rhyne TL. Acoustic propagation properties of normal, stunned, and infarcted myocardium. Morphological and biochemical determinants. *Circulation* 1995; **91**: 154–160.
35. Wickline SA, Verdonk ED, Sobel BE, Miller JG. Identification of human myocardial infarction in vitro based on the frequency dependence of ultrasonic backscatter. *J Acoust Soc Am* 1992; **91**: 3018–3025.
36. Wickline SA, Verdonk ED, Wong AK, Shepard RK, Miller JG. Structural remodeling of human myocardial tissue after infarction. Quantification with ultrasonic backscatter. *Circulation* 1992; **85**: 259–268.
37. Hall CS, Verdonk ED, Wickline SA, Perez JE, Miller JG. Anisotropy of the apparent frequency dependence of backscatter in formalin fixed human myocardium. *J Acoust Soc Am* 1997; **101**: 563–568.
38. Iwahashi M, Muragaki Y, Ooshima A, Umesaki N. Decreased type I collagen expression in human uterine cervix during pregnancy. *J Clin Endocrinol Metab* 2003; **88**: 2231–2235.
39. Bigelow TA, McFarlin BL, O'Brien WD Jr, Oelze ML. In vivo ultrasonic attenuation slope estimates for detecting cervical ripening in rats: Preliminary results. *J Acoust Soc Am* 2008; **123**: 1794–1800.
40. Wear KA, Stiles TA, Frank GR, Madsen EL, Cheng F, Feleppa EJ, Hall CS, Kim BS, Lee P, O'Brien WD Jr, Oelze ML, Raju BI, Shung KK, Wilson TA, Yuan JR. Interlaboratory comparison of ultrasonic backscatter coefficient measurements from 2 to 9 MHz. *J Ultrasound Med* 2005; **24**: 1235–1250.
41. Yao LX, Zagzebski JA, Madsen EL. Backscatter coefficient measurements using a reference phantom to extract depth-dependent instrumentation factors. *Ultrason Imaging* 1990; **12**: 58–70.
42. Kuc R. Bounds on estimating the acoustic attenuation of small tissue regions from reflected ultrasound. *Proc IEEE* 1982; **73**: 1159–1168.
43. Lu ZF, Zagzebski JA, Lee FT. Ultrasound backscatter and attenuation in human liver with diffuse disease. *Ultrasound Med Biol* 1999; **25**: 1047–1054.
44. Oosterveld BJ, Thijssen JM, Hartman PC, Romijn RL, Rosenbusch GJ. Ultrasound attenuation and texture analysis of diffuse liver disease: methods and preliminary results. *Phys Med Biol* 1991; **36**: 1039–1064.
45. Parker KJ, Tuthill TA, Baggs RB. The role of glycogen and phosphate in ultrasonic attenuation of liver. *J Acoust Soc Am* 1988; **83**: 374–378.
46. Zderic V, Keshavarzi A, Andrew MA, Vaezy S, Martin RW. Attenuation of porcine tissues in vivo after high-intensity ultrasound treatment. *Ultrasound Med Biol* 2004; **30**: 61–66.
47. Lu ZF, Zagzebski JA, O'Brien RT, Steinberg H. Ultrasound attenuation and backscatter in the liver during prednisone administration. *Ultrasound Med Biol* 1997; **23**: 1–8.
48. Schmitz G, Ermert H, Senge T. Tissue-characterization of the prostate using radio frequency ultrasonic signals. *IEEE Trans Ultrason Ferroelectr Freq Control* 1999; **46**: 126–138.
49. Tavakoli MB, Evans JA. Dependence of the velocity and attenuation of ultrasound in bone on the mineral content. *Phys Med Biol* 1991; **36**: 1529–1537.
50. Wear KA. Ultrasonic attenuation in human calcaneus from 0.2 to 1.7 MHz. *IEEE Trans Ultrason Ferroelectr Freq Control* 2001; **48**: 602–608.
51. Lee KI, Roh HS, Yoon SW. Correlations between acoustic properties and bone density in bovine cancellous bone from 0.5 to 2 MHz. *J Acoust Soc Am* 2003; **113**: 2933–2938.
52. Cook RB, Collins D, Tucker J, Zioupos P. The ability of peripheral quantitative ultrasound to identify patients with low bone mineral density in the hip or spine. *Ultrasound Med Biol* 2005; **31**: 625–632.
53. Tuthill TA, Baggs RB, Parker KJ. Liver glycogen and water storage: effect on ultrasound attenuation. *Ultrasound Med Biol* 1989; **15**: 621–627.
54. Tuthill TA, Baggs RB, Violante MR, Parker KJ. Ultrasound properties of liver with and without particulate contrast agents. *Ultrasound Med Biol* 1991; **17**: 231–237.
55. Bigelow TA, O'Brien WD Jr. A Model for estimating ultrasound attenuation along the propagation path to the fetus from backscattered waveforms *J Acoust Soc Am* 2005; **118**: 1210–1220.
56. Mamou J, Oelze ML, O'Brien WD Jr, Zachary JF. Identifying ultrasonic scattering sites from three-dimensional impedance maps. *J Acoust Soc Am* 2005; **117**: 413–423.
57. Mamou J, Oelze ML, O'Brien WD Jr, Zachary JF. Three-dimensional acoustic tissue model: a computational tissue phantom for imaging analyses. *Acoustical Imaging* 2007; **28**: 419–426.
58. Mamou J, Oelze ML, O'Brien WD Jr, Zachary JF. Extended three-dimensional impedance map methods for identifying ultrasonic scattering sites. *J Acoust Soc Am* 2008; **123**: 1195–1208.
59. Oelze ML, O'Brien WD Jr. Frequency-dependent attenuation-compensation functions for ultrasonic signals backscattered from random media. *J Acoust Soc Am* 2002; **111**: 2308–2319.
60. Oelze ML, O'Brien WD Jr. Defining optimal axial and lateral resolution for estimating scatterer properties from volumes using ultrasound backscatter. *J Acoust Soc Am* 2004; **115**: 3226–3234.
61. Oelze ML, Zachary JF, O'Brien WD, Jr. Parametric imaging of rat mammary tumors in vivo for the purposes of tissue characterization. *J Ultrasound Med* 2002; **21**: 1201–1210.
62. Oelze ML, Zachary JF, O'Brien WD Jr. Characterization of tissue microstructure using ultrasonic backscatter: theory and technique for optimization using a Gaussian form factor. *J Acoust Soc Am* 2002; **112**: 1202–1211.

